# STAR experiment results from Beam Energy Scan program

Alexey Aparin for the STAR collaboration*

*Joint Institute for Nuclear Research, 6 Joliot-Curie St.,*

*Dubna, Moscow Region, Russia, 141980*

## Abstract

The STAR experiment at RHIC has been put into operation more than two decades ago and since then has provided unique data on relativistic heavy-ion collisions. One of the main topics of interest for STAR's experimental program is related to the transition from regular hadronic matter to the quark-gluon plasma state. To shed light on the mechanism of such transition and its exact location on the QCD phase diagram, RHIC has performed two phases of the Beam Energy Scan program lowering collision energy from 200 GeV to 3 GeV. Large-statistics samples obtained during BES-II program at both collider and fixed-target modes allow us to possibly locate the phase boundary and the Critical Point.

This report will summarize results obtained from BES-I and new results from some of the BES-II energies. These results can help shape the physics programs of new experiments in the field (MPD@NICA, CBM@FAIR, JPARC).

PACS numbers: 13.85.–t; 14.20.–c; 25.75.–q

*e-mail:aparin@jinr.ru

## I. INTRODUCTION.

After discovering that the QCD matter under extreme conditions of high temperature and baryonic density undergoes a phase transition into a new state of strongly interacting Quark Gluon Plasma (QGP), relativistic heavy ion physics has been aiming at investigating this phenomenon and searching for the exact location of the phase boundary. On top of that, theoretical calculations from lattice QCD suggested the phase transition at top RHIC and LHC energies (low baryon chemical potential $\mu_B \approx 0$) to be a smooth crossover [1], yet at lower collision energies (at high $\mu_B$) the first-order phase transition should take place, implying the existence of the Critical Point (CP) where these regimes meet [2], [3]. The STAR experiment launched a special Beam Energy Scan (BES) program for detailed investigations of the QCD phase structure during 2010 - 2021. The first phase of this program provided experimental data on Au+Au collisions in energy range $7.7 - 62.4$ GeV, but was limited by both detector and accelerator capabilities providing limited statistics especially at the lowest collision energy. The second stage of BES program was successfully performed in period 2017 - 2021 after several major upgrades of RHIC and STAR which allowed to increase available statistics by a factor $\approx 100$ and extend the energy reach down to $\sqrt{s_{NN}} = 3$ GeV by taking data in the Fixed-Target (FXT) mode. Main detector upgrades for the BES-II included a full replacement of the inner part of STAR Time Projection Chamber (TPC), installation of the end-cap Time-of-Flight (TOF) system and the Event Plane Detector (EPD) which was put into operations in 2018. Those upgrades significantly increased the detector acceptance and tracking capabilities. Figure I demonstrates identification capabilities with TPC (top) and TOF (bottom) systems for the 3 GeV FXT mode in 2018 before the upgrade.

In this proceedings, we report the beam energy dependence of various observables based on BES-I and part of BES-II data: identified particle and hyper-nuclei production, light nuclei flow, femtoscopic measurements, di-lepton production. This systematic measurement of collision energy dependence for different observables will help search for the phase transition and CP in the QCD phase diagram.

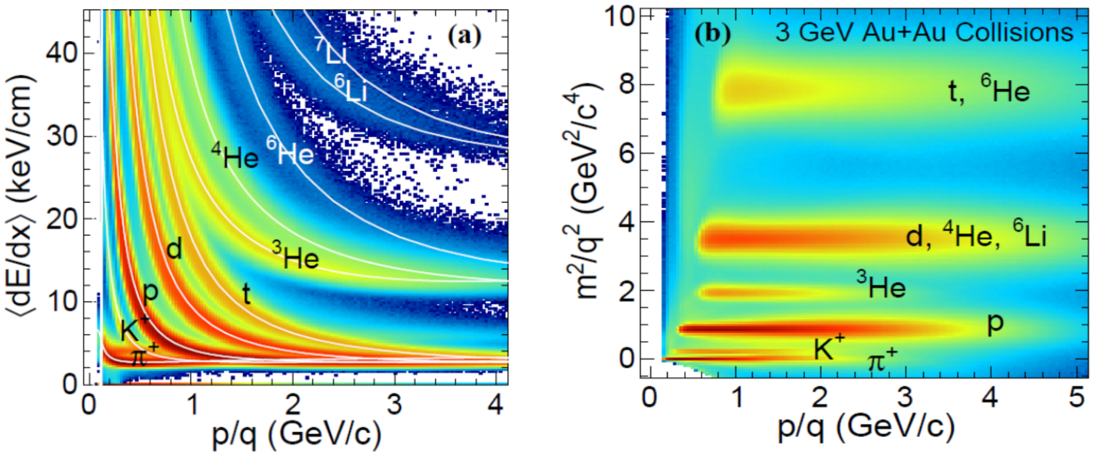


FIG. 1: STAR particle identification capabilities at 3 GeV before the BES-II detector upgrade. (a) Dependence of particle energy loss on its rigidity $p/q$. The curves are Bichsel expectations for the labeled particle species. (b) Dependence od particle $m^2/q^2$ on rigidity $p/q$.

## II. PARTICLE PRODUCTION

The QCD phase diagram is usually plotted in terms of temperature $T$ and baryon chemical potential $\mu_B$ or net baryon density $n$. If we assume the system produced in heavy ion collisions (HIC) is in thermalization, both variables, and thus different areas of the phase diagram, can be accessed by varying the collision energy. This scan over phase diagram was the primary goal of two phases of BES program at RHIC which started in 2010 and was completed in 2021. Table I lists the statistics recorded by the STAR experiment during this program with a reference baryon chemical potential for each collision energy.

Figure II shows the comparison of $K^{*0}$ and $\phi$ to kaon ratios as a function of event centrality based on the BES-I data [4]. This ratio can help understand the interactions during the hadronic phase of the medium since the lifetime of $K^{*0}$ is comparable to that of the medium and therefore its decay daughters can undergo re-scatterings with medium and get decorrelated or medium particles can recombine and form new $K^{*0}$. On the other hand, the $\phi$-meson has a much longer lifetime and thus not affected by the hadronic phase. As shown in Fig. II, the $K^{*0}/K$ ratio decreases from peripheral to central collisions, indicating the dominance of re-scattering over regeneration in central collisions, while for $\phi/K$ no significant collision energy dependence is seen. The high statistics data from BES-II will allow more precise measurements of hadronic resonances at energies 19.6 GeV and below.

TABLE I: Minimum bias statistics acquired by the STAR experiment in the beam energy scan program during 2010 - 2021.

| $\sqrt{s_{NN}}$ GeV | Data taking mode | Number of minimum bias events | $\mu_B$ MeV |
|---|---|---|---|
| 62.4 | BES-I | 67M | 73 |
| 54.4 | BES-II | 1.2B | 90 |
| 39 | BES-I | 39M | 112 |
| 27 | BES-I/BES-II | 70M/555M | 156 |
| 19.6 | BES-I/BES-II | 36M/582M | 206 |
| 17.3 | FXT | 256M | 230 |
| 14.6 | BES-II | 324M | 262 |
| 14.5 | BES-I | 20M | 264 |
| 13.7 | FXT | 52M | 276 |
| 11.5 | BES-I/BES-II/FXT | 12M/235M/50M | 315 |
| 9.2 | BES-I/BES-II/FXT | 300K/162M/50M | 372 |
| 7.7 | BES-I/BES-II/FXT | 4M/100M/262M | 420 |
| 7.2 | FXT | 472M | 443 |
| 6.2 | FXT | 118M | 487 |
| 5.2 | FXT | 103M | 541 |
| 4.5 | FXT | 108M | 589 |
| 3.9 | FXT | 117M | 633 |
| 3.5 | FXT | 116M | 665 |
| 3.2 | FXT | 200M | 699 |
| 3.0 | FXT | 2.3B | 720 |

Measurements of $K^{*0}/K$ ratio in a broad beam energy range can provide information on production mechanisms, especially the energy dependence of the relative strength of re-scattering and regeneration processes. A suppression of $K^{*0}/K$ ratio was observed in central HIC relative to the small system collisions. This smaller $K^{*0}/K$ ratio compared to small system collisions makes the dominance of re-scattering over regeneration in the most central heavy ion collisions the most preferable description of the data. The high statistics

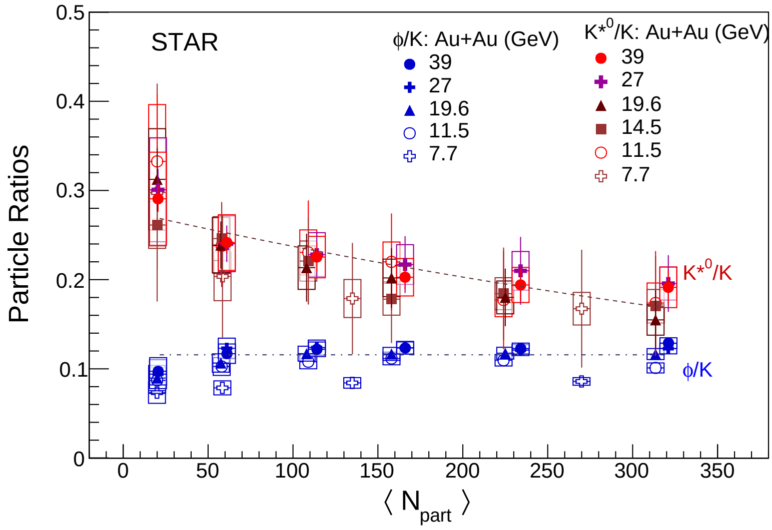


FIG. 2: Systematic study of strange particle ratios as a function of participating nucleons. $K^{*0}$ to kaon ratio demonstrates a smooth decrease with the increase of the number of participating nucleons. $\phi$-meson to kaon ratio on the contrary does not show such a dependence. The trend is similar for all investigated collision energies.

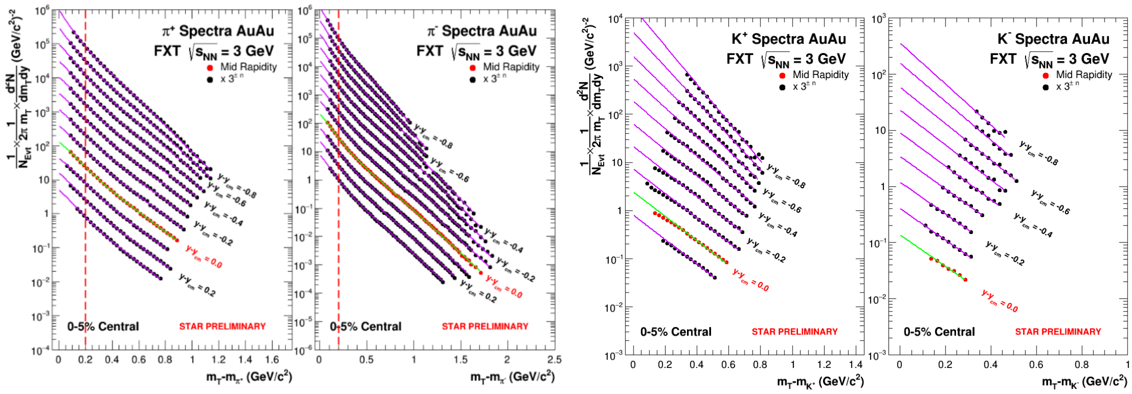


FIG. 3: Transverse mass $m_T$ spectra of charged pions (left panel) and charged kaons (right panel) for different rapidity intervals in 3 GeV Au+Au collisions. Double Boltzmann function is used to describe the pion production, while an exponential function is used to fit the kaon spectrum. Dashed red lines show the location where the leading production mechanism for pions changes.

data from the BES-II will allow more precise measurements of hadronic resonances at these energies.

Figure III demonstrates the first results on transverse mass dependence of pion and kaon yields in Au+Au collisions at $\sqrt{s_{NN}} = 3$ GeV. Different groups of data points correspond to different rapidity intervals. These spectra are used to obtain the rapidity distributions of corresponding particles. The integration over unmeasured $m_T$ region is done by fitting the spectra with double Boltzmann function for pions [5] and with an exponential function for kaons [6]

$$\frac{1}{2\pi m_T}\frac{d^2N}{dm_T dy} = A m_T \exp-(m_T - m_0)/T_1 + A m_T \exp-(m_T - m_0)/T_2 \tag{1}$$

$$\frac{1}{2\pi m_T}\frac{d^2N}{dm_T dy} = A \exp-(m_T - m_0)/T \tag{2}$$

In HIC at such low energy, baryon stopping causes a non-negligible net positive charge in the interaction region, which can modify the spectra of particles through the Coulomb interaction. The Coulomb potential should affect positively and negatively charged pions in the opposite ways, shifting $\pi^+$ to higher $m_T$ and $\pi^-$ to lower $m_T$.

Production of strange particles at such low energies is different than at high energies and it was argued that the Canonical Ensemble (CE) should be used instead of the Grand Canonical Ensemble (GCE). The collision energy of 3 GeV is just above the $\phi$-meson production threshold which makes it very sensitive to the exact production mechanism of strangeness.

Figure IV shows ratios of strange particle yields $\phi/K^-$ and $\phi/\Xi$ as a function of collision energy including data from AGS, SPS and RHIC [7]. Measured ratios at $\sqrt{s_{NN}} = 3$ GeV are compatible or higher than those at higher energies despite the near-threshold production of $\phi$ and below-threshold production of $\Xi$. Strange particle ratios indicate the thermal phase space at low energies is far from the GCE limit and the local treatment of strangeness conservation is crucial.

## III. HYPERNUCLEI PRODUCTION

Figure V shows the comparison of world data on measured lifetimes for ${}^3_\Lambda H$ and ${}^4_\Lambda H$ from different experiments [9]. STAR has measured the lifetime to be is 221$\pm$ 15($stat.$)$\pm$ 19($syst.$) ps for ${}^3_\Lambda H$ using FXT Au+Au collisions at $\sqrt{s_{NN}} = 3$ and 7.2 GeV and 218 $\pm$ 6($stat.$) $\pm$ 13($syst.$) ps for ${}^4_\Lambda H$. Results for both hypernuclei are noticeably different from the lifetime of free $\Lambda$ baryon. High statistics data collected by STAR during BES-II will allow to extend these measurements for heavier hypernuclei and their antiparticles. Measurement of lifetime

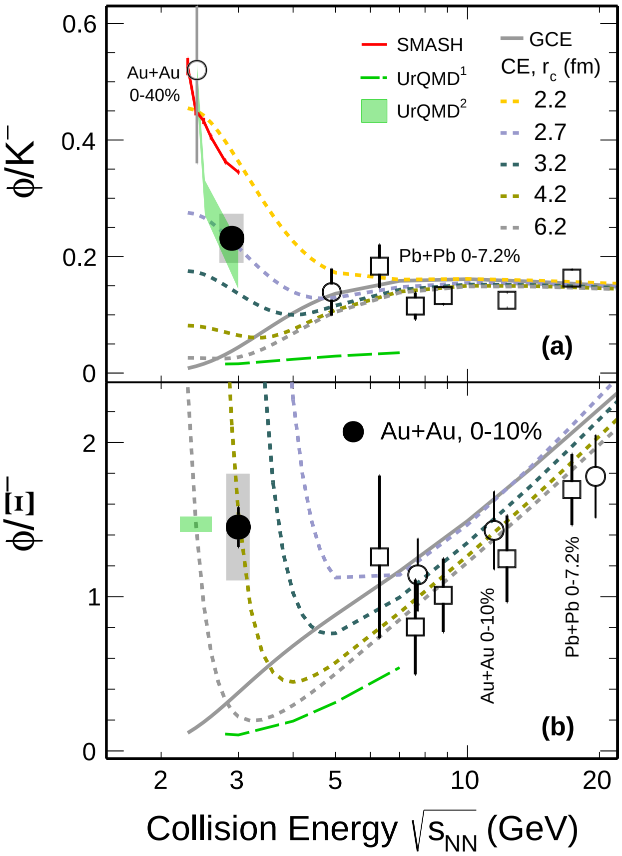


FIG. 4: Ratios of $\phi$-meson to $K^-$ (a) and $\Xi^-$ (b) as a function of collision energy. The solid black circles show the results in 0-10% central Au+Au collisions at 3 GeV. The grey solid lines represent model predictions based on the Grand Canonical Ensemble (GCE), while the dotted lines depict calculations based on the Canonical Ensemble (CE) with different values of the strangeness correlation radius.

and mass differences between hypernuclei and corresponding anti-hypernuclei will provide a unique opportunity to test the validity of fundamental CPT symmetry in the hypernuclei sector. Further measurements based on the high statistics data from BES-II for ${}^{3}_{\Lambda}\bar{H}$, ${}^{4}_{\Lambda}\bar{H}$ and possibly ${}^{4}_{\Lambda}\bar{H}e$ will help to perform such tests for a variety of hypernuclei species.

Transverse momentum spectra of hypernuclei were measured for central $0-10\%$ and mid-central $10-50\%$ Au+Au collisions at 3 GeV for different rapidity intervals. The $p_T$-integrated yields of ${}^{3}_{\Lambda}H$ and ${}^{4}_{\Lambda}H$ at mid-rapidity were calculated for central collisions as a function of center-of-mass energy. It demonstrated a significant enhancement compared to the results at 2.76 TeV from ALICE experiment [10], which can be explained by the increase

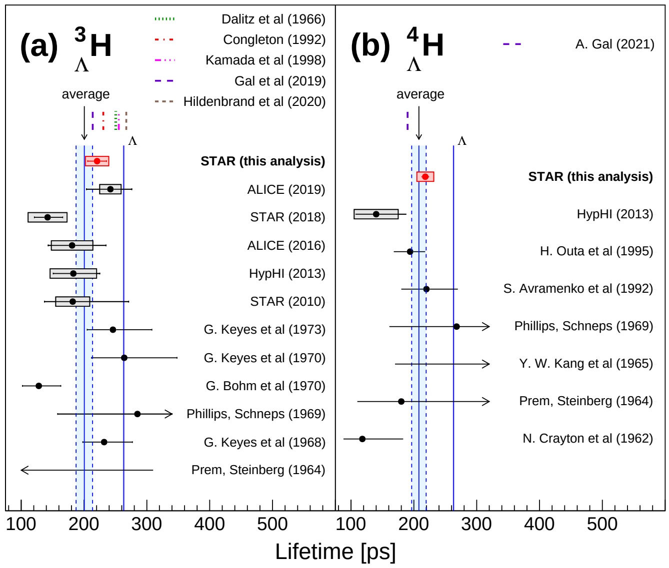


FIG. 5: Measured lifetimes of $^{3}_{\Lambda}H$ and $^{4}_{\Lambda}H$ from different experiments. Horizontal lines represent statistical uncertainties, while boxes represent systematic uncertainties. Vertical blue bands represent the average lifetimes of $^{3}_{\Lambda}H$ and $^{4}_{\Lambda}H$ and free $\Lambda$ baryon. Data are taken from the paper [9].

in baryon density at low energies. The result was compared to several model predictions. The thermal model with the canonical ensemble for strangeness [11] can describe the yields of $^{3}_{\Lambda}H$ at both 3 GeV and 2.76 TeV, while it underestimates the yield for $^{4}_{\Lambda}H$ at 3 GeV. Coalescence calculations using Dubna Cascade Model (DCM) give good agreement for $^{3}_{\Lambda}H$ yields and underestimate $^{4}_{\Lambda}H$ production, whereas the coalescence calculations with JAM model are consistent with both at 3 GeV.

## IV. FLOW

Anisotropy in collective motion of produced particles has been observed in early HIC experiments [12]-[14]. It is a general phenomenon that can be quantified by the Fourier decomposition of the azimuthal distribution of particles produced in the collision along the collision symmetry plane [15]:

$$E\frac{d^3N}{dp^3} = \frac{1}{2\pi}\frac{d^2N}{p_T dp_T d\eta}(1 + \Sigma 2 v_n cos[n(\phi - \Psi_n)]) \tag{3}$$

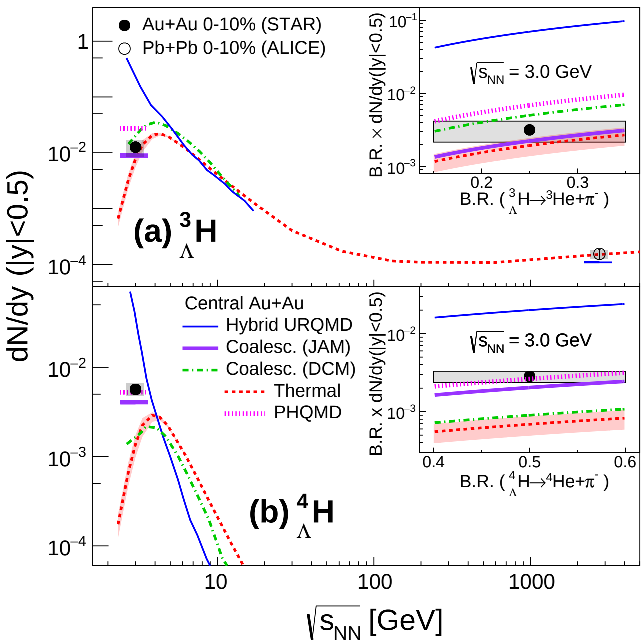


FIG. 6: Dependence of ${}^3_\Lambda H$ and ${}^4_\Lambda H$ yields within $|\eta| < 0.5$ on the beam energy in $0-10\%$ central heavy-ion collisions. The symbols represent STAR measurements while the lines represent different theoretical calculations.

where $p_T$, y, $\phi$ and $\Psi$ are particle transverse momentum, rapidity, azimuthal angle and the event plane angle, respectively. The first two coefficients, called directed flow $v_1$ and elliptic flow $v_2$, are widely used for studying the properties of the sQGP [12], [13]. Large positive $v_2$, especially for multistrange hadrons, along with the observation of its number-of-constituent quarks (NCQ) scaling are strong evidence for the formation of hydrodynamically expanding partonic QCD matter.

The STAR collaboration has previously reported the atomic mass number ($A$) scaling of light nuclei $v_2$ for the reduced transverse momentum $p_T$ range of $p_T/A < 1.5$ GeV/c at $\sqrt{s_{NN}} = 7.7 - 200$ GeV [20] which can be written in the following form

$$v_n^A(p_T, y)/A \approx v_n^p(p_T/A, y). \tag{4}$$

This behavior favors the coalescence as the main production mechanism for nuclei in HIC. At low energies, $v_1$ values for light nuclei are measured to be non-negligible, and Eq. 4 for $n = 2$ becomes:

$$v_2^A(p_T, y)/A \approx v_2^p(p_T/A, y) + \frac{A-1}{2}\left(v_1^p(p_T/A, y)\right)^2 \tag{5}$$

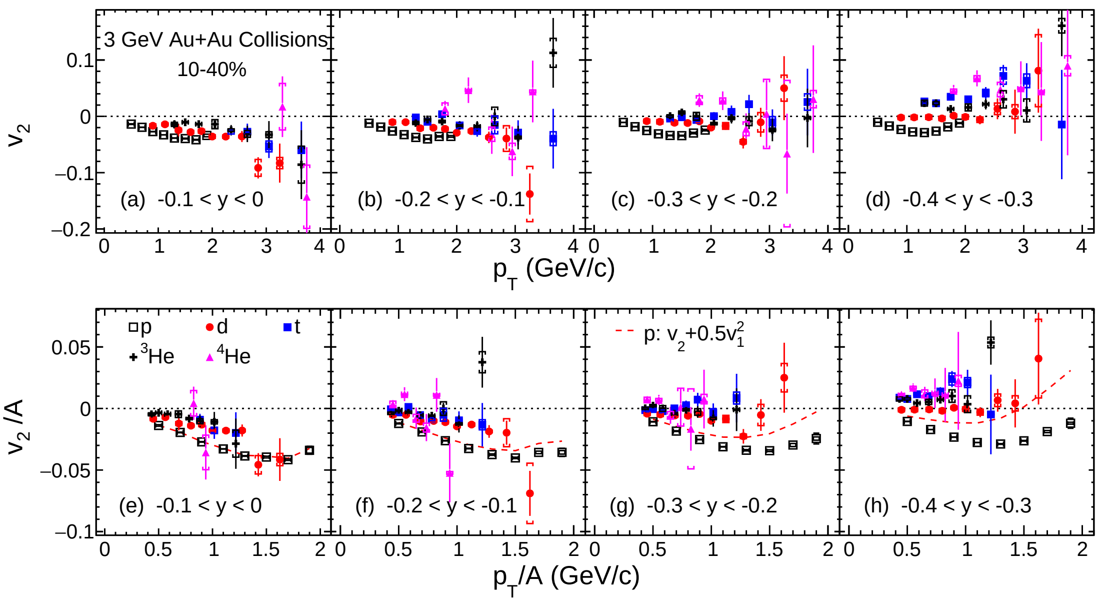


FIG. 7: Transverse momentum dependence of $v_2$ for $p$, $d$, $t$, $^3$He and $^4$He in $10-40\%$ mid-central Au+Au collisions at 3 GeV (top panel) for different rapidity intervals. Same results scaled by corresponding nuclear mass number $A$ (bottom panel).

The coalescence model implies the formation of light nuclei through the combination of nucleons that are near each other both in coordinate and momentum phase space near the time of kinetic freeze-out [16] - [18]. As spectator nucleons strongly affect the flow, measurements of light nuclei flow coefficients $v_1$ and $v_2$ will provide new insight into the collision dynamics and the nucleon coalescence behavior at low collision energies.

Figure VII shows transverse momentum dependence of $v_2$ for $p$, $d$, $t$, $^3$He and $^4$He in different rapidity intervals [19]. The magnitude of $v_2$ grows steadily from negative values for all nuclei species at mid-rapidity $-0.1 < y < 0$ to positive values for $t$, $^3$He and $^4$He at rapidity $-0.4 < y < -0.3$, while for $p$ and $d$ it stays negative. It is also seen that $v_2$ has a stronger non-monotonic dependence on $p_T$ for protons compared to other light nuclei. Lower panels of the Fig. VII show $v_2$ scaled to mass number $A$. It is seen that the scaling is broken and different nuclei do not follow the same trend as obtained before for $\sqrt{s_{NN}} = 7.7 - 200$ GeV [20].

These results collaborate with recent measurements of $\pi, K$ amd $p$ $v_2$ at $\sqrt{s_{NN}} = 3$ GeV made by the STAR experiment [21]. The value of elliptic flow coefficient scaled by the number of constituent quarks was measured as a function of the scaled transverse kinetic energy $(m_T - m_0)/n_q$. Unlike the famous NCQ-scaling obtained at higher STAR energies $\sqrt{s_{NN}} = 7.7 - 200$ GeV [22], [23] for both positive and negative particles, at 3 GeV all of the values of $v_2/n_q$ are negative.

The NCQ scaling observed at RHIC for collision energies $\sqrt{s_{NN}} = 7.7{-}200$ GeV originates from partonic collectivity, which was one of the important evidences for the QGP formation. At energy $\sqrt{s_{NN}} = 3$ GeV partonic interactions no longer dominate and baryonic scatterings take over, which means hadronic matter is predominantly created in such collisions. Particles and antiparticles no longer follow the single-particle NCQ scaling due to the mixture of the transported and produced quarks. The negative $v_2$ at mid-rapidity may be caused by shadowing of the spectators as their passage time is comparable with the expansion time of the compressed system. Similar results were reported by the HADES collaboration [24].

## V. PARTICLE FEMTOSCOPY

A standard method for studying the space and time characteristics of the emitting source created in heavy ion collisions is the two-particle interferometry, also referred to as the femtoscopy [25]. Combination of meson and baryon femtoscopy measurements provide complementary information about the source in the final states of interactions.

Figure VIII shows dependences of pion-pion correlation function on the three components (out, side, long) of the pair momentum. Measured distributions are fitted with the Lednicky-Luboshitz function [26]. Correlation functions can be further used to extract the values of correlation radii $R_{out}, R_{side}, R_{long}$ for the pion emission source.

Figure IX shows correlation functions of identical deutron pairs for different centralities, and a mild centrality dependence is seen. Those were further compared to the Lednicky-Luboshitz function with different source sizes. Presented results indicate that the source size could depend on collision centrality or the effect of final state interactions needs to be taken into account.

## VI. DI-LEPTON RESULTS

One more independent tool to investigate the properties of the QGP is the electromagnetic probes. Electromagnetic probes, i.e. leptons and photons, are emitted at different stages

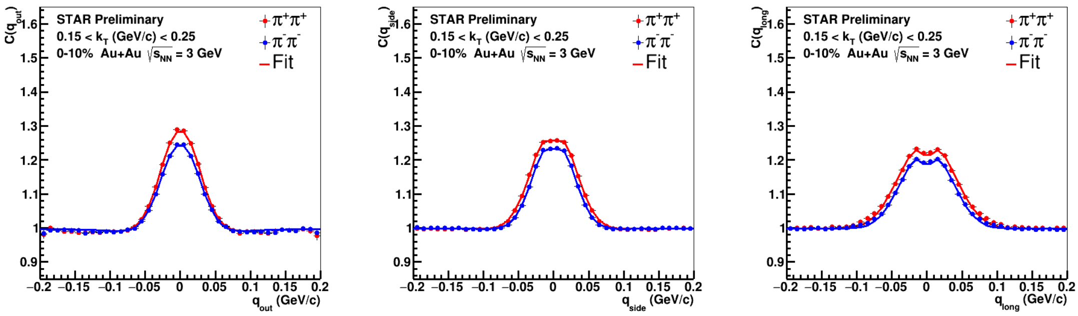


FIG. 8: Correlation function of pair of identical pions for out, side and long components of the pair momenta (from left to right)in 0-10% most central Au+Au collisions at 3 GeV. Fit is done with Lednicky-Luboshitz function.

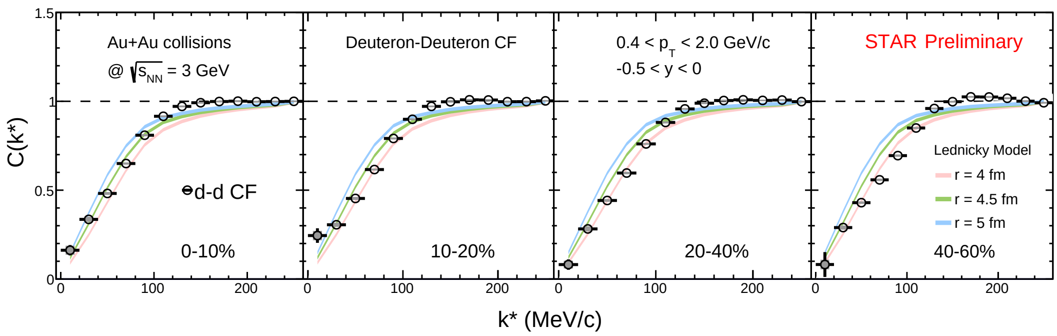


FIG. 9: Correlation function of pair of deutron-deutron as a function of pair momentum for different centralities in Au+Au collisions at 3 GeV. Solid lines represent different emitting source radii in the Lednicky-Luboshitz model.

of the HIC. Because they do not participate in the strong interaction they can preserve the initial information of the produced medium throughout the fireball evolution. Invariant mass spectrum of thermal dileptons carries the temperature information of both QGP and hadronic phases. The Low Mass Region (LMR, $M_{ee} < 1.1$ GeV/c$^2$) can be used to extract the temperature of the hadronic medium, whereas the Intermediate Mass Region (IMR, $M_{ee} > 1.1$ GeV/c$^2$) can be used to extract the temperature of the QGP.

Figure X shows the phase diagram mapping based on electromagnetic probes measured by STAR, HADES and NA60 experiments. IMR temperature $T^{IMR}$ reaches about 300 MeV

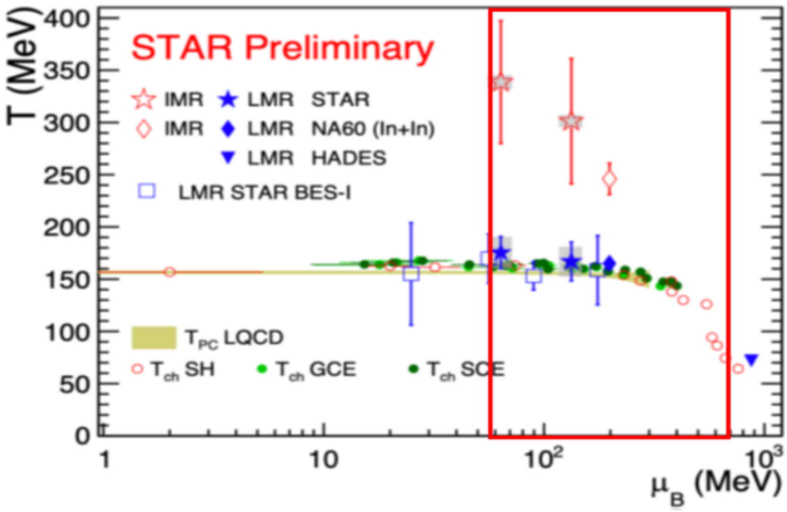


FIG. 10: Measurements of the medium temperature based on the invariant mass spectra of dileptons from STAR, HADES and NA60 experiments as a function of baryon chemical potential $\mu_B$. Red rectangle represents the area accessible with BES-II data.

at collision energies of $\sqrt{s_{NN}} = 27, 54.4$ GeV (low $\mu_B$ region). Measured LMR temperature $T^{LMR} \approx 170$ MeV provides the first experimental evidence that in-medium $\rho$-meson is dominantly produced around the phase transition temperature. BES-II statistics will allow precise measurements of dileptons in the kink area of the phase diagram, indicated by the red box in Figure X.

## VII. SUMMARY

In the year 2021, the STAR experiment collected the final data sets of the BES program, which spans over a decade, for experimental investigations of the phase structure of the QCD matter produced in heavy ion collisions. Data collected in the collider mode with energy $\sqrt{s_{NN}} = 7.7 - 54.4$ GeV combined with FXT data $\sqrt{s_{NN}} = 3 - 7.7$ GeV cover the region in $\mu_B \approx 90 - 720$ MeV. Detector upgrades, high statistics and the vast range of collision energies will allow STAR to perform precise measurements of different observables which are believed to be sensitive to the phase transition from regular hadron matter to sQGP phase and possible effects of the Critical Point which marks the change in phase transition type from a cross-over to the first order phase transition.

## Acknowledgments

Author would like to acknowledge that part of the work described in section II on particle production was supported by Russian Science Foundation under grant N 22-72-10028.

---

[1] Karsch F. et al. [E895 Collaboration], Nucl. Phys. B Proc. Suppl. 129, 614, (2004)
[2] J. Cleymans and K. Redlich, Phys. Rev. C 60, 054908, (1999).
[3] A. Andronic, P. Braun-Munzinger, and J. Stachel, Nucl. Phys. A 772, 167, (2006).
[4] arXiv:2210.02909v1 [nucl-ex]
[5] Karsch F. et al. [E895 Collaboration], Phys. Rev. C 68, 054905, (2003).
[6] T. Anticic et al. [NA49 collaboration], Phys. Rev. C 84, 064909, (2011).
[7] M. S. Abdallah et al., [STAR Collaboration], Phys. Lett. B 831, 137152, (2022).
[8] J. Steinheimer, K. Gudima, A. Botvina, I. Mishustin, M. Bleicher, and H. Stocker, Phys. Lett. B 714, 85, (2012).
[9] M. S. Abdallah et al., [STAR Collaboration], Phys. Rev. Lett. 128, 202301, (2022).
[10] J. Adam et al. [ALICE collaboration], Phys. Lett. B 754, 360, (2016).
[11] A. Andronic et al., Phys. Lett. B 697, 203, (2011).
[12] C. M. Hung and E. V. Shuryak, Phys. Rev. Lett. 75, 4003, (1995).
[13] J. Steinheimer, et al., Phys. Rev. C 89, 054913, (2014).
[14] K. Aamodt et al. [ALICE Collaboration], Phys. Rev. Lett. 105, 252302, (2010).
[15] A. M. Poskanzer and S. A. Voloshin, Phys. Rev. C 58, 1671, (1998).
[16] S. T. Butler and C. A. Pearson, Phys. Rev. 129, 836, (1963).
[17] H. Sato and K. Yazaki, Phys. Lett. B 98, 153, (1981).
[18] S. Zhang, et al., Phys. Lett. B 684, 224, (2010).
[19] M. S. Abdallah et al., [STAR Collaboration], Phys. Lett. B 827, 136941, (2022).
[20] L. Adamczyk et al. [STAR Collaboration], Phys. Rev. C 94, 034908, (2016).
[21] M. S. Abdallah et al., [STAR Collaboration], Phys. Lett. B 827, 137003, (2022).
[22] X. Dong, S. Esumi, P. Sorensen, N. Xu, and Z. Xu, Phys. Lett. B 597, 328, (2004).
[23] L. Adamczyk et al., [STAR Collaboration], Phys. Rev. C 88, 014902, (2013).
[24] J. Adamczewski-Musch et al. [HADES Collaboration], Phys. Rev. Lett. 125, 262301, (2020).

[25] M. Lisa, S. Pratt, R. Soltz and U. Wiedemann, Ann. Rev. Nucl. Part. Sci. 55, 357, (2005).

[26] R. Lednicky and V. L. Lyuboshitz, Sov. J. of Nucl. Phys. 35, 770, (1982).